

JPMTR 089 | 1614  
DOI 10.14622/JPMTR-1614  
UDC 620-024-035.56

Research paper  
Received: 2016-11-08  
Accepted: 2016-12-27

## Designed structures for bone replacement

*Azem Yahamed<sup>1</sup>, Pavel Ikononov<sup>2</sup>, Paul D. Fleming<sup>1</sup>, Alexandra Pekarovicova<sup>1</sup> and Peter Gustafson<sup>3</sup>*

<sup>1</sup> Department of Chemical and Paper Engineering,  
Western Michigan University, Kalamazoo, MI 49008

E-mails: azemkhalifa.yahamed@wmich.edu  
pavel.ikononov@wmich.edu  
dan.fleming@wmich.edu  
a.pekarovicova@wmich.edu  
peter.gustafson@wmich.edu

<sup>2</sup> Department of Engineering Design Manufacturing,  
and Management Systems,  
Western Michigan University, Kalamazoo, MI 49008

<sup>3</sup> Department of Mechanical Engineering,  
Western Michigan University, Kalamazoo, MI 49008

### Abstract

Bone replacements are needed to help repair or replace damaged and diseased tissues ranging from trauma, degenerative disease, cancer and plastic surgery requirements. To create artificial bone implants from plastics, the structure and mechanical properties must be tested to closely match or be able to sustain greater forces than the original. It is essential to use proper bone replacement material that provides biocompatibility with sufficient stiffness and strength. The materials can be biocompatible polymers, such as polylactic acid (PLA), polyvinyl alcohol (PVA), polycaprolactone (PCL) and polyether-ether ketone (PEEK). Also, it is important to create internal structures that can accurately mimic the real human bone structure with a solid outer shell that represents the compact bone and porous internal volume that represents the trabecular (spongy) bone. Designing of the proper trabecular bone is one of the most critical steps, because its structure helps support the entire bone, while at the same time reduces the weight. Due to the low resolution of DICOM images, the trabecular bone structures cannot be obtained directly from CT and MRI scans. Therefore, we used CAD software – SolidWorks to design special 3D structures (hexagonal, triangular, and square). The reason for using these structures is that they are widely used in industry and aerospace applications, because they provide high strength, while keeping the weight low. The geometry of the void structure reduces the amount of material, reducing the overall weight and cost by reducing the structural density. We designed and produced 3D printed samples to test the structure properties with different geometric shapes. Structure property tests, such as tensile strength test, compressive strength test, and bending test were investigated. We found that the mechanical properties of the designed plastic structures either exceed or fall within the range of the mechanical properties of the human trabecular bones.

**Keywords:** mechanical property, 3D printing, biomaterial, bone structure

## 1. Introduction

Designed void structures, with their unique design properties providing mechanical strength and light weight, have attracted massive attention lately for both fundamental research and practical applications and progressively have become a hot research area (Heng et al., 2013). These structures have great properties, such as high mechanical strength, excellent structural stability, large space area, and low density. For example, the honeybee comb is one of the natural cellular structures that has been investigated by several groups of researchers: physicists, mathematicians, and biologists. The microstructure of the walls and the macroscopic properties of honeybee combs have been researched in

depth. The natural honeybee comb has been a typical example of interest for engineered cellular structures (Heng et al., 2013).

### 1.1 Three-dimensional printing

Three-dimensional printing technology is able to create 3D items by using many different materials. The technology is also called rapid prototyping, because it is a programmed process where 3D items are rapidly made (Tyagi, 2011). Building 3D models using 3D printing technology saves time and cost because designing, manufacturing, and assembling of separate parts of a

product are not required. The technology of 3D printing can make models of objects either designed with Computer Aided Design (CAD) programs or scanned with 3D scanners. The technology has been widely used in many applications such as industrial design, engineering, architecture, aerospace, dental and medical applications (Tyagi, 2011).

One of the uses of 3D printing in the medical field is to substitute for damaged bones. For example, the 3D printing technology has been already applied to replace the bone structure of the injured or missing parts of people's skulls damaged by diseases or trauma (Ehrenberg, 2013). There are many cases when the bone structure is extensively damaged and cannot be recovered with regular methods, such as casts. Currently, damaged bones are repaired with metal parts, but many cases show that the bone cannot be properly replaced or repaired. However, there have been several successful attempts of using 3D printing to create and replace human bone structures even for most complex shapes, such as jaws (Bahat and Fontanessi, 2001). Many different biocompatible and biodegradable materials have been studied and tested for 3D printed bone structure. There are different 3D printing methods that can be applied for bone tissue-engineering: Fused Deposition Modeling (FDM) (Ahn et al., 2002), Selective Laser Sintering (SLS) (Materialise, 2016), and stereolithography (Yahamed et al., 2016).

### 1.2 Thermoplastics

Thermoplastics have been used successfully as replacements for certain metals for many years in manufacturing, and recently they have been used widely in medical applications. Polymer 3D printing plays a significant role in applying these materials, providing high performance, cost efficiency and enhanced resistance to environmental conditions (Jia and Kagan, 2001).

## 2. Methods

### 2.1 Three-dimensional printing of test samples

Using 3D printing technology, three different 3D printed samples of plastic materials were printed; ULTEM9085, PA2200, and Digital ABS™ were employed. Table 1 shows selected properties of these plastics.

### 1.3 Biomaterials

The study of biomaterials for bone replacement has progressed significantly over many years (Stevanovic et al., 2013). There are many examples of applications of 3D printing in creating implantable organs that are designed for specific patients to enhance accuracy and efficiency of the manufacturing. Three-dimensional printing uses computer models to build 3D objects by printing layers of materials, including plastics, metals, powders and liquid layer by layer. The process is also used to build items in the medical field that can exactly match the requirements and sizes of specific patients (Yahamed et al., 2015).

### 1.4 Bioprinting

Three-dimensional printing can improve medical care in some processes, and it will also open new opportunities for bone replacement or cure. For example, this technology has been successfully applied in the field of prosthetics and drug printing (Miller, 2013). Constructive processes are used to produce 3D models, and 3D printing refers to only such technologies that use constructive manufacturing procedures. It is likely that more medical professionals will introduce 3D printing technologies into their practices; 3D printing gives enormous benefits for experts to produce only what they need, which can reduce production time. It allows objects from actual human scans to be modeled and built for further applications in a few hours, even inside medical facilities (Miller, 2013). Several processes can be accomplished only with the use of a 3D printer. Biofabrication is a process that doctors themselves traditionally use to produce organ replacements or order them from specialized companies. However, they can now be more successfully realized by using 3D printing technologies (Yahamed et al., 2015).

We used SolidWorks software to design the internal engineered structure with different geometric shapes (hexagonal, triangular, and square). The samples were printed using different 3D printing methods (Yahamed et al., 2016). The FDM technique was used to print ULTEM9085 (Stratasys, 2015), with Stratasys machine

Table 1: Selected properties of thermoplastic materials specified by their producers

Material	Tensile strength (MPa)	Young's modulus (MPa)	Melting point (°C)
ULTEM9085	71.6	2200	186
PA2200	48.0	1700	172–180
Digital ABS™	55.0–60.0	2600–3000	47–53*

\* Glass transition temperature ( $T_g$ ), since this material cannot be crystallized.

Fortus 400 MC, and SLS was used to print PA2200 with EOSP 396 (EOS, 2015). PolyJet™ technology was used to print Digital ABS™ with a Stratasys Objet 500 Connex3 (Stratasys, 2016). All the samples were printed with designed internal structures with different geometric shapes. Five samples were printed for each category. Although Digital ABS™ is not a biocompatible material, it is used as a reference for comparison with other polymers. From the biocompatible materials, ULTEM9085 is helpful as a tissue engineering scaffold for bone regeneration (Tao and Young, 2006), and PA2200 (polyamide) can be used in several medical applications such as compressed structures for scaffold supporting (Stoia, Vigar and Rusu, 2015). In this work, we mimic the trabecular (spongy) bone structure with the average pore size of the real one (~400  $\mu\text{m}$ ). The designed structures are shown in Figures 1 to 3.

## 2.2 Testing mechanical properties of 3D printed samples using MTS machine

The tested samples were designed according to the standard with specific dimensions for all mechanical property tests. The following standards were employed: for tensile strength ISO 3167 (International organization for Standardization, 2014), for compression ASTM D695 (ASTM International, 2015a), and for bending

ASTM D790 (ASTM International, 2015b). An MTS Bionix Servohydraulic Test Systems Model 370.02 instrument was employed for testing. We tested the 3D printed samples at 0.2 mm/s speed of MTS machine at room temperature. The force capacity of the device is 25 kN and it is used to determine the dynamic properties for a number of biomaterials. The axial alignments of the system are intended to achieve precise tension, compression and bending tests as well as fatigue and fracture studies. Also, they are used to test durability properties of components such as hip, knee and spine implants (Yahamed et al., 2016).

## 2.3 Calculating void volume and percentage of infill for designed structures

We calculated the void volume and percentage of infill for the designed structures with different geometric shapes. Table 2 shows the void volume fraction, fill fraction and percentage of infill for the geometric shapes. We wanted to investigate the influence of the geometry shape on the percentage of infill and the impact of the percentage of infill on the strength. From Table 2, we observe that the hexagonal structure has the highest percentage of infill (92.6%), followed by the triangular structure (83.6%), and the lowest infill has the square structure (82.9%).

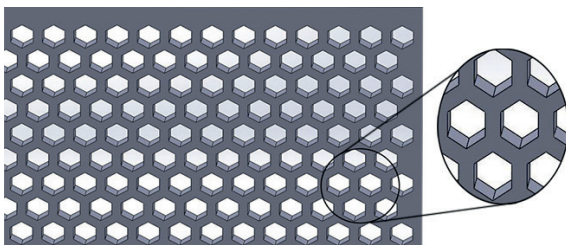


Figure 1: Hexagonal structure

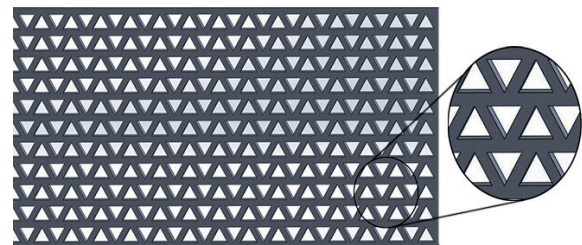


Figure 2: Triangular structure

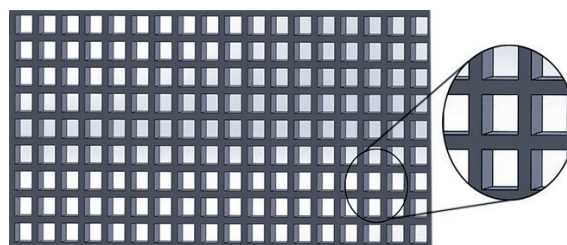


Figure 3: Square structure

Table 2: Void volume fraction, fill fraction and percentage of infill for designed structures

Geometric structure	Void volume fraction	Fill fraction	Infill (%)
Square	0.172	0.829	82.9
Triangular	0.164	0.836	83.6
Hexagonal	0.074	0.926	92.6

### 3. Results and discussion

#### 3.1 Tensile strength tests

Table 3 shows the results of the average tensile strength and Young's modulus for ULTEM9085, PA2200, and Digital ABS™ geometric structures after testing with the MTS machine, compared to values of corresponding solid samples. In all cases, the structures (see Figures 1 to 3) are perpendicular to the tension direction and parallel to the Z direction.

The ULTEM9085 polymer printed with three different geometries, hexagonal, triangular and square, gave the same values for the tensile strength, but different Young's modulus values (Table 3). The triangular structure has the highest Young's modulus, followed by square structure, and the lowest Young's modulus was found in ULTEM9085 hexagonal structure.

The hexagonal structure of PA2200 has the highest tensile strength average and Young's modulus (Table 3), followed by PA2200 square structure and triangular structure. For Digital ABS™, the square structure has the highest average value for both tensile strength and Young's modulus, followed by hexagonal structure and triangular structure. Generally, the values are in the same range for all the structures. However, if we look at hexagonal structure, the PA2200 resulted in highest tensile strength (43 MPa) along with highest Young's modulus (1 508 MPa). Similarly, ULTEM9085 resulted in the strongest triangular structure, with Young's modulus of 1 480 MPa and tensile strength of 32 MPa. Triangular structure of ULTEM9085 had slightly higher Young's modulus (1 480 MPa) than that of PA2200 (1 456 MPa). The strongest square struc-

ture with the highest tensile strength of 43 MPa and Young's modulus of 1 487 MPa.

Figure 4 shows Young's modulus vs. tensile strength for designed structures. Tensile strength is the capacity of the material or structure to withstand loads tending to elongate. Tested 3D printed polymer structures show particular trend in values. There is significant relation between Young's modulus and tensile strength and the correlation is close to linear.

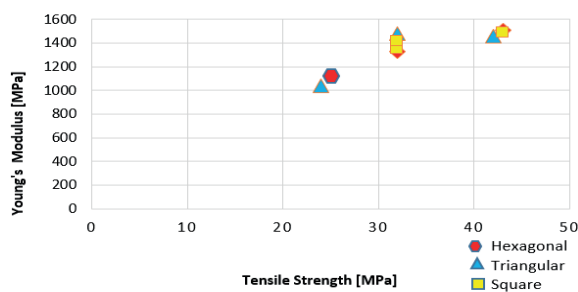


Figure 4: Young's modulus vs. tensile strength for tested materials and structures

Figure 5 shows the stress-strain curves calculated from the least squares fit to the tensile data for ULTEM9085 hexagonal, triangular, and square structures at the MTS machine speed of 0.2 mm/s and room temperature.

Similarly, the stress-strain curves calculated from the least squares fit to the tensile data for PA2200 and Digital ABS™ structures were obtained, as given in Figures 6 and 7, respectively. The curves exhibit near linear trend, showing that the rupture occurs without

Table 3: The values and standard deviations of tensile strength and Young's modulus for different geometric structures; standard deviation of Young's modulus was calculated from the standard error of the coefficient of the linear term in a quadratic fit to the tensile data

Geometric structure	Tensile strength (MPa)	SD (MPa)	Young's modulus (MPa)	SD (MPa)
<b>ULTEM9085 solid</b>	49.7	0.6	1 540	3
ULTEM9085 hexagonal	32.0	3.0	1 327	10
ULTEM9085 triangular	32.0	2.0	1 480	11
ULTEM9085 square	32.0	1.0	1 347	3
<b>PA2200 solid</b>	49.7	0.7	1 699	12
PA2200 hexagonal	43.0	3.0	1 508	17
PA2200 triangular	42.0	3.0	1 456	15
PA2200 square	43.0	2.0	1 487	4
<b>Digital ABS™ solid</b>	55.0	3.0	2 013	12
Digital ABS™ hexagonal	24.7	0.6	1 124	3
Digital ABS™ triangular	23.8	0.5	1 036	3
Digital ABS™ square	32.0	3.0	1 414	15

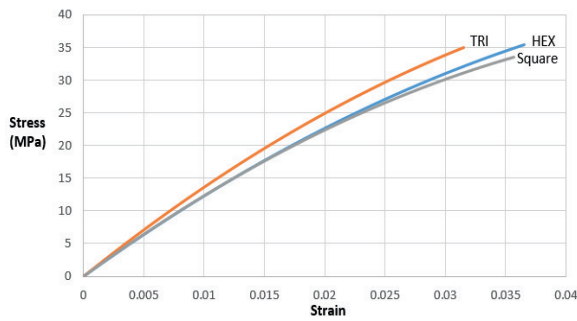


Figure 5: ULTEM9085 structures stress-strain calculated from tensile data

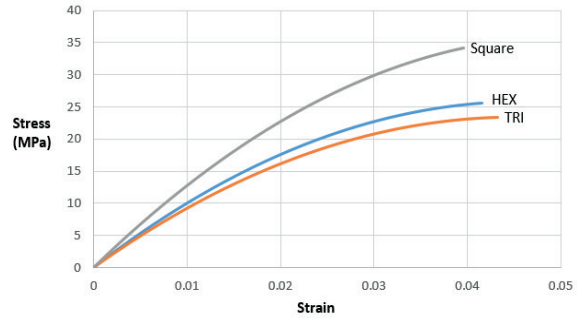


Figure 7: Digital ABS™ structures stress-strain calculated from tensile data

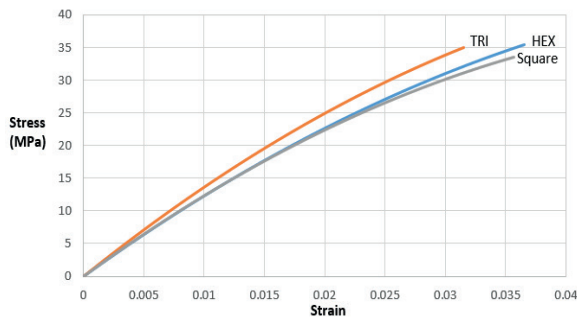


Figure 6: PA2200 structures stress-strain calculated from tensile data

any dramatic change in elongation, which is typical for brittle structures (Beer et al., 2012).

Figure 6 shows the stress-strain curves for PA2200 structures. The shape of the stress strain curves pinpoints brittle structures, which do not exhibit any dramatic change in elongation prior to rupture. Figure 7 shows the stress-strain curves for Digital ABS™

geometric structures, which show a stress-strain trend of brittle structures. The brittle material ruptures without any obvious prior change in the rate of elongation.

Table 4 shows the tensile breaking energy and energy per unit strain per unit mass for different geometric structures of the materials, along with values of corresponding solid samples. From Table 4, PA2200 square has the highest value for both tensile energy per unit strain per unit mass, and breaking energy per unit mass. After that PA2200 triangular is the second. Then PA2200 hexagonal is the third. The PA2200 breaking energy values for both triangular and square are almost indistinguishable from the 100 % infill case for this polymer. This is an indication that these two structures can absorb about the same tensile energy per unit mass as the corresponding solid structure without failing. This could have a profound effect in using this polymer for replacements of original components in many applications. Digital ABS™ hexagonal has the lowest values for both tensile energy per unit strain per unit mass and breaking energy per unit mass.

Table 4: The values and standard deviations of tensile breaking energy and energy per unit mass per unit strain for designed structures

Geometric structure	Breaking energy per unit mass (kJ/kg)	SD (kJ/kg)	Energy per unit mass absorbed per unit strain (kJ/kg)	SD (kJ/kg)
<b>ULTEM9085 solid</b>	37.3	0.4	1 149	2
ULTEM9085 hexagonal	25.8	2.4	1 070	8
ULTEM9085 triangular	28.6	1.8	1 321	10
ULTEM9085 square	28.8	0.9	1 203	3
<b>PA2200 solid</b>	121.0	2.0	3 951	28
PA2200 hexagonal	108.0	8.0	3 789	43
PA2200 triangular	117.0	8.0	4 044	42
PA2200 square	119.0	5.0	4 130	11
<b>Digital ABS™ solid</b>	47.0	3.0	1 706	10
Digital ABS™ hexagonal	23.0	1.0	1 028	3
Digital ABS™ triangular	24.0	1.0	1 050	3
Digital ABS™ square	33.0	3.0	1 446	13

### 3.2 Compressive strength

Compressive strength tests provide information about the compressive properties of geometric structures. The compressive test properties explain the performance of the material with its internal engineered structure when it is compressed under a load that is relatively low and uniform. Compressive strength of trabecular bones is in the range of 5 MPa to 10 MPa (Razak, Sharif and Rahman, 2012).

The specimen dimensions were printed as blocks according to ASTM D695 standard. Table 5 shows the results of the compressive strength and compressive modulus for selected materials from material safety data sheets (MSDS).

Table 5: Compressive strength and compressive modulus for selected materials from MSDS

Material	Compressive strength (MPa)	Compressive modulus (MPa)
ULTEM9085	104	1 930
PA2200	58	1 500
Digital ABS™	70	2 200

Table 6 shows the average compressive strength and compressive modulus for ULTEM9085, PA2200, and Digital ABS™ structures and corresponding solid samples after testing with the MTS machine.

Table 6 shows that all the materials have compressive strength sufficient for replacement of trabecular bones. The compressive modulus is the highest for Digital ABS™ hexagonal structure, followed by ULTEM 9085

triangular and square structures. On the other hand, compressive strength values were indistinguishable among PA2200 structures and ULTEM9085 square and triangular structures. The least compressive strength was found for Digital ABS™ hexagonal structures, which had the highest compressive modulus.

For brittle materials, the eventual strength in compression is much higher than the eventual strength in tension. This refers to the existence of microscopic cracks or cavities, which tend to deteriorate the material in tension, while not significantly affecting its resistance to compressive failure (Beer et al., 2012).

Figure 8 shows compressive strength vs. compressive modulus for the designed structures. Compressive strength is the capacity of the material or structure to resist loads tending to decrease in size differently than when under tensile strength, which resists loads tending to elongate. Roughly, Figure 8 shows a random relation between compressive strength and compressive modulus of chosen polymer 3D structures, as confirmed by statistical analysis.

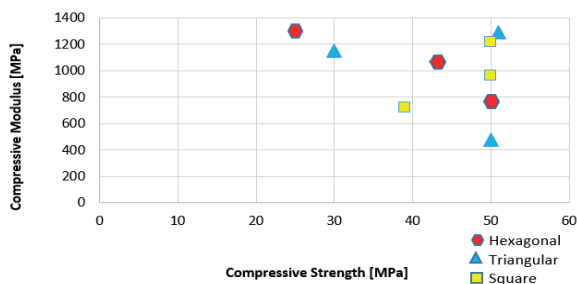


Figure 8: Compressive modulus vs. compressive strength for tested materials and structures

Table 6: The values and standard deviations of compressive strength and compressive modulus for various geometries; standard deviation of compressive modulus was calculated from the standard error of the coefficient

Geometric structure	Compressive strength (MPa)	SD (MPa)	Compressive modulus (MPa)	SD (MPa)
<b>ULTEM9085 solid</b>	69.98	0.05	1 870	13
ULTEM9085 hexagonal	42.98	0.02	1 068	13
ULTEM9085 triangular	50.98	0.02	1 293	16
ULTEM9085 square	49.99	0.02	1 216	4
<b>PA2200 solid</b>	54.93	0.15	1 175	23
PA2200 hexagonal	49.99	0.01	763	10
PA2200 triangular	49.70	0.60	476	4
PA2200 square	49.70	0.70	962	13
<b>Digital ABS™ solid</b>	75.00	5.00	2 157	20
Digital ABS™ hexagonal	25.00	3.00	1 298	10
Digital ABS™ triangular	29.99	0.01	1 153	11
Digital ABS™ square	39.00	1.00	716	7

Compressive modulus values of human trabecular bone range from 1 MPa to 5000 MPa, with strength values ranging from 0.10 MPa to 27.3 MPa (Williams et al., 2005). The plastics structures show compressive modulus values ranging from 476 MPa to 1298 MPa. The strength values of the plastic structures range from 25 MPa to 60 MPa. The compressive moduli values fall within the range of human trabecular bone, while the compressive strength values exceed the range of human trabecular bone. Figure 9 shows the stress-strain curves calculated from least squares fit to compression data for ULTEM9085 geometric structures.

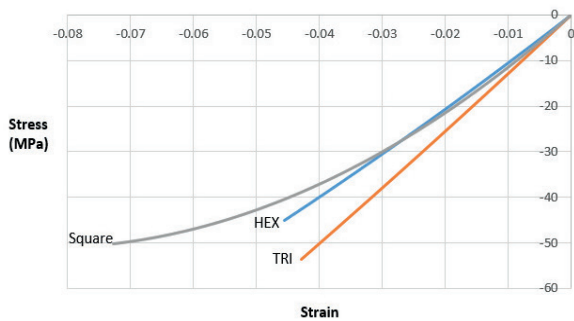


Figure 9: ULTEM9085 structures stress-strain calculated from fit to compression data

Figure 10 shows the stress-strain curves of PA2200 geometric structures under the compression test. The hexagonal and square PA2200 structures appear to have convex trend while triangular PA2200 structure shows concave trend.

Figure 11 shows the stress-strain curve calculated from least squares fit to compression data for Digital ABS™ geometric structures.

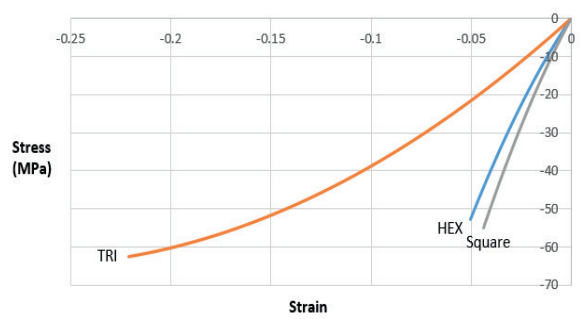


Figure 10: PA2200 structures stress-strain calculated from fit to compression data

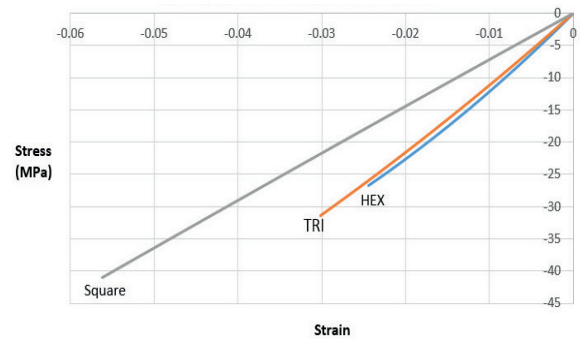


Figure 11: Digital ABS™ structures stress-strain calculated from fit to compression data

Table 7 shows the breaking energy per unit mass and energy per unit mass per unit strain for the different geometric structures of the materials, compared to values of corresponding solid samples. From Table 7, PA2200 square has the highest compressive energy per unit strain value per unit mass. Then, PA2200 hexagonal is the second and PA2200 triangular is the third,

Table 7: The values and standard deviations of compressive breaking energy and energy per unit mass per unit strain for designed structures

Geometric structure	Breaking energy per unit mass (kJ/kg)	SD (kJ/kg)	Energy per unit mass per unit strain (kJ/kg)	SD (kJ/kg)
<b>ULTEM9085 solid</b>	52	0.04	1396	10
ULTEM9085 hexagonal	35	0.02	861	10
ULTEM9085 triangular	46	0.02	1155	14
ULTEM9085 square	45	0.02	1096	3
<b>PA2200 solid</b>	121	34.00	2733	53
PA2200 hexagonal	126	0.02	1917	25
PA2200 triangular	139	2.00	1322	11
PA2200 square	140	2.00	2702	36
<b>Digital ABS™ solid</b>	64	4.00	1828	16
Digital ABS™ hexagonal	23	3.00	1188	9
Digital ABS™ triangular	30	0.01	1168	11
Digital ABS™ square	40	1.00	732	7

while Digital ABS™ square has the lowest compressive energy per unit strain per unit mass. Further, PA2200 square has the highest compressive breaking energy per unit mass, with Digital ABS™ hexagonal having the lowest. All of the various void structures for PA2200 seem to be able to absorb more compressive energy per unit mass than the corresponding solid structure.

### 3.3 Bending strength

Bending strength tests measure the force required to bend a beam under three-point loading conditions. The goal of this test is to select materials for parts that should support loads without flexing. A homogeneous, isotropic material would have identical tensile and bending strengths. More flexible polymers have lower bending strength values than stiffer ones (MatWeb, 2016). However, printed 3D polymer structures are not expected to be isotropic; the polymer chains may be oriented in the print direction, which ultimately gives non-isotropic character to the structure.

On the macroscopic level, non-isotropic character is created by selection of the particular structure. The flexural modulus indicates the stiffness of material depending on its internal structure when bent. Flexural or bending modulus would ideally have the same value as compressive or tensile modulus, but it often differs, especially for polymers. The load is applied to the center generating three-point bending at a certain rate. The test parameters are the support span, loading rate, and the determined deflection. They all are based on the specimen thickness and are defined by ASTM D790 standard. Table 8 shows the flexural strength and flexural modulus of the selected materials from their MSDS.

Table 8: Flexural strength and flexural modulus for selected materials from MSDS

Material	Flexural strength (MPa)	Flexural modulus (MPa)
ULTEM9085	115	2500
PA2200	58	1500
Digital ABS™	66–75	1700–2200

Table 9 shows the average flexural strength and flexural modulus for ULTEM9085, PA2200, and Digital ABSTM structures after testing with the MTS machine, as well as values of corresponding solid samples.

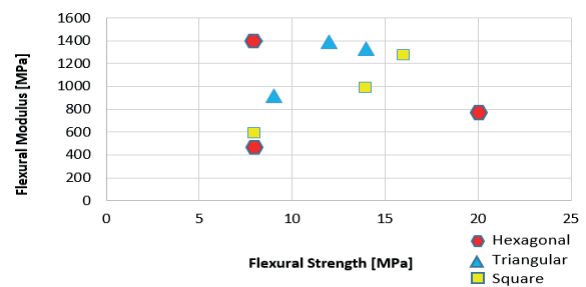


Figure 12: Flexural modulus vs. flexural strength for tested materials and structures

Figure 12 shows the relationship between flexural strength and flexural modulus of 3D printed polymer structures, showing no particular trend in values. The behavior between flexural strength and flexural modulus follows a random relation. There is no significant relation between flexural strength and flexural modulus, as confirmed by statistical analysis. Hexagonal Digital ABS™ and square Digital ABS™ structure with 8 MPa

Table 9: The values and standard deviations of flexural strength and flexural modulus for structures; standard deviation of flexural modulus was calculated from the standard error of the coefficient of the linear term in a quadratic fit to the bending data

Geometric structure	Flexural strength (MPa)	SD (MPa)	Flexural modulus (MPa)	SD (MPa)
<b>ULTEM9085 solid</b>	30.00	1.00	2049	20
ULTEM9085 hexagonal	19.89	0.22	767	3
ULTEM9085 triangular	12.00	2.00	1390	5
ULTEM9085 square	13.99	0.01	983	4
<b>PA2200 solid</b>	29.93	0.14	1490	30
PA2200 hexagonal	7.99	0.01	1400	15
PA2200 triangular	13.64	0.73	1331	13
PA2200 square	15.96	0.08	1270	12
<b>Digital ABS™ solid</b>	20.00	5.00	1120	8
Digital ABS™ hexagonal	7.87	0.26	465	8
Digital ABS™ triangular	8.89	0.21	915	10
Digital ABS™ square	8.84	0.32	590	10

bending strength have a much lower flexural modulus (465 MPa and 590 MPa) than PA2200 hexagonal structure with the same bending strength, but much higher flexural modulus of 1400 MPa. Overall, all PA2200 structures had flexural modulus over 1000 MPa.

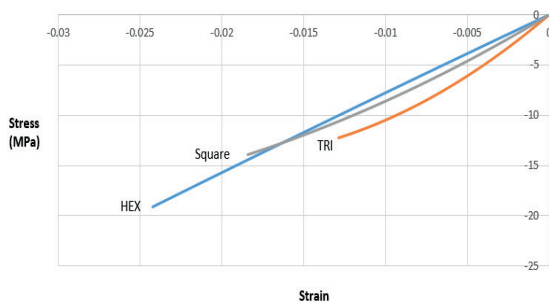


Figure 13: ULTEM9085 structures stress-strain calculated from fit to bending data

Figure 13 shows the stress-strain curve calculated fit to bending data for ULTEM9085 geometric structures at an MTS machine speed of 0.2 mm/s at room temperature. The hexagonal structure appears convex for ULTEM9085, while triangular and square structures appear concave. Figure 14 shows the stress-strain curve calculated least squares fit to bending data for PA2200 geometric structures. All the structures appear to have a concave trend. Figure 15 shows the stress-strain curve calculated from least squares fit to bending data for Digital ABS™ structures, with concave character as well.

Table 10 shows the flexural breaking energy per unit mass and energy per unit mass per unit strain for different geometric structures of the materials, along with values of corresponding solid samples. From Table 10, PA2200 triangular has the highest flexural energy per unit strain value per unit mass, after that PA2200

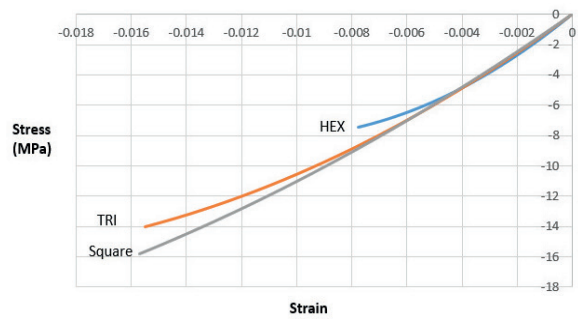


Figure 14: PA2200 structures stress-strain calculated from fit to bending data

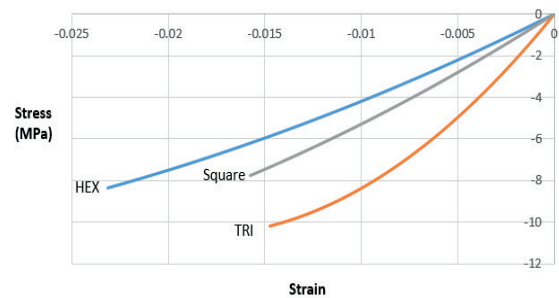


Figure 15: Digital ABS™ structures stress-strain calculated from fit to bending data

square has the second highest and PA2200 hexagonal the third. Digital ABS hexagonal has the lowest values for both flexural energy per unit strain per unit mass and flexural breaking energy per unit mass. The flexural strength per unit mass for the PA2200 square is not quite as much as the corresponding solid structure, but it is stiffer on a mass basis than the solid structure. This indicates that as long as the structure doesn't fail, it will bend less under moderate forces than the corresponding solid structure having the same mass.

Table 10: The values and standard deviations of flexural breaking energy and energy per unit mass per unit strain for designed structures

Geometric structure	Breaking energy per unit mass (kJ/kg)	SD (kJ/kg)	Energy per unit mass per unit strain (kJ/kg)	SD (kJ/kg)
<b>ULTEM9085 solid</b>	22.4	0.70	1 529	15
ULTEM9085 hexagonal	16.0	0.18	619	2
ULTEM9085 triangular	10.7	1.80	1 241	4
ULTEM9085 square	12.6	0.10	886	3
<b>PA2200 solid</b>	69.8	0.30	3 465	70
PA2200 hexagonal	20.0	0.03	3 517	37
PA2200 triangular	39.0	2.00	3 697	36
PA2200 square	44.8	0.22	3 576	33
<b>Digital ABS™ solid</b>	17.0	4.00	949	7
Digital ABS™ hexagonal	7.3	0.24	425	7
Digital ABS™ triangular	9.1	0.21	927	10
Digital ABS™ square	8.2	0.32	603	10

#### 4. Conclusion

From the tensile results, the highest Young's modulus for ULTEM9085 was obtained with the triangular structure and the lowest value was obtained with the hexagonal structure. The tensile strength test values are the same for all three structures of ULTEM9085, but lower than the solid value. For PA2200, hexagonal structure has the highest value of Young's modulus, while the triangular structure has the lowest, although they are not that much different from one another. For Digital ABS™, the square structure has the highest values for both Young's modulus and tensile strength, while the triangular structure has the lowest values for both. The relationship between tensile strength and Young's modulus is well correlated.

For the compressive test, the highest values are obtained with the triangular structure and the lowest ones are obtained with the hexagonal structure for ULTEM9085. For PA2200, the square structure has the highest compressive modulus and the triangular has the lowest compressive modulus, but the tensile strengths are the same for all three structures. For Digital ABS™ the hexagonal structure has the highest compressive modulus value but the lowest compressive strength. The square structure has the lowest compressive modulus but the highest compressive strength. This indicates that the compressive modulus is acting contrary with compressive strength for this polymer. The eventual strength in compression is higher than the eventual strength in tension for brittle materials. This is because the existence of microscopic cracks or cavities, which tend to deteriorate the material in tension, while not significantly affecting its resistance to compressive failure. However, the microcracked compressed sample will likely not return to its original shape, which would compromise its behavior to additional stresses.

For the bending test, the ULTEM9085 triangular structure has the highest value of flexural modulus, but the lowest bending strength value, whereas ULTEM9085 hexagonal structure has the lowest value of flexural modulus, but has the highest bending strength. The hexagonal structure of PA2200 showed the highest flexural modulus value, but the lowest bending strength. The square structure showed the lowest flexural modulus value, but the highest bending strength. Digital ABS™ triangular structure has the highest flexural modulus value and the highest bending strength. The hexagonal structure for Digital ABS™ has the lowest flexural modulus. The highest bending strength was obtained with the triangular structure, while the hexagonal and square structures have the same bending strength values. The behavior between flexural strength and flexural modulus follow random

relation, with no significant correlation between flexural strength and flexural modulus.

The square structure of PA2200 has the highest values for both tensile energy per unit strain per unit mass and tensile breaking energy per unit mass. After that PA2200 triangular is the second and PA2200 hexagonal is the third. The PA2200 tensile breaking energy values for both triangular and square are virtually indistinguishable from the 100 % infill case for this polymer. This is an indication that these two structures can absorb about the same tensile energy per unit mass as the corresponding solid structure without failing. Digital ABS™ hexagonal has the lowest values for both tensile energy per unit strain and tensile breaking energy per unit mass.

Further, PA2200 square also has the highest compressive energy per unit strain value per unit mass. Then, PA2200 hexagonal is the second and PA2200 triangular is the third, while Digital ABS™ square has the lowest compressive energy per unit strain per unit mass. Moreover, PA2200 square has the highest compressive breaking energy per unit mass and Digital ABS™ hexagonal has the lowest compressive strength value per unit mass. All of void structures for PA2200 seem to be able to absorb more compressive energy per unit mass than the corresponding solid structure.

Finally, PA2200 triangular has the highest flexural breaking energy value per unit mass. After that PA2200 square has the second highest flexural breaking energy value per unit mass and PA2200 hexagonal has the third. Digital ABS™ hexagonal has the lowest values for both flexural breaking energy per unit mass and flexural energy absorbed per unit strain per unit mass. The flexural strength per unit mass for the PA2200 square is not quite as much as the corresponding solid structure, but it is stiffer on a mass basis than the solid structure. This indicates that as long as the structure doesn't fail, it will bend less under moderate forces than the corresponding solid structure having the same mass.

From the results, it is hard to identify which structure is the strongest and has the best mechanical properties. This is because the 3D printed samples of the structures were printed using different 3D printing methods of the printed materials. The results of the thermoplastic designed structures either exceed or fall within the range of the mechanical properties of the human trabecular bone. However, the PA2200 shows the most promise for all of the void structures. It would be even more interesting if the behavior reported here could be replicated using other printing methods such as FDM or inkjet.

## References

- Ahn, S.-H., Montero, M., Odell, D., Roundy, S. and Wright, P.K., 2002. Anisotropic material properties of fused deposition modeling ABS. *Rapid Prototyping Journal*, 8(4), pp. 248–257.
- ASTM International, 2015a. *ASTM D695-15 Standard Test Method for Compressive Properties of Rigid Plastics*. Westconchocken, PA: ASTM International.
- ASTM International, 2015b. *ASTM D790-15e2 Standard Test Method for Flexural Properties of Unreinforced and Reinforced Plastics and Electrical Insulating Materials*. Westconchocken, PA: ASTM International.
- Bahat, O. and Fontanessi, R.V., 2001. Implant placement in three-dimensional grafts in the anterior jaw. *International Journal of Periodontics & Restorative Dentistry*, 21(4), pp. 357–365.
- Beer, F.P., Johnston, E.R., DeWolf, J.T. and Mazurek, D.F., 2012. *Mechanics of Materials*. New York: McGraw Hill Companies.
- Ehrenberg, R., 2013. Health & Illness: Skull patched with plastic. *Science News*, 183(8), p. 12.
- EOS, 2015. *Material data sheet: PA 2200*. [pdf] EOS GmbH – Electro Optical System. Available at: <[https://www.shapeways.com/rstatic/material\\_docs/mds-strongflex.pdf](https://www.shapeways.com/rstatic/material_docs/mds-strongflex.pdf)> [Accessed September 2015].
- Heng, L., Wang, B., Li, M., Zhang, Y. and Jiang, L., 2013. Advances in fabrication materials of honeycomb structure films by the breath-figure method. *Materials*, 6(2), pp. 460–482.
- International Organization for Standardization, 2014. *ISO 3167:2014 – Plastics – Multipurpose test specimens*. Geneva: ISO.
- Jia, N. and Kagan, V.A., 2001. Mechanical performance of polyamides with influence of moisture and temperature – accurate evaluation and better understanding. In: J. Moalli, ed. 2001. *Plastic Failure Analysis and Prevention*. Norwich, NY: William Andrew Inc. pp. 95–104.
- MatWeb, 2016. *Flexural Strength Testing of Plastics*. [online] Available at: <<http://www.matweb.com/reference/flexuralstrength.aspx>> [Accessed November 2016].
- Materialise, 2016. *Stereolithography*. [online] Available at: <<http://manufacturing.materialise.com/stereolithography>> [Accessed 15 January 2016].
- Miller, M.B., 2013. *Applications of 3D Printing in the Medical Field*. [e-book] Smashwords Inc. Available through: Smashwords Inc. website: <<https://www.smashwords.com/books/view/327956>> [Accessed 1 February 2016].
- Razak, S.I.A., Sharif, N.F.A. and Rahman, W.A.W.A., 2012. Biodegradable polymers and their bone applications: a review. *International Journal of Basic & Applied Sciences IJBAS IJENS*, 12(1), pp. 31–49.
- Stevanovic, S., Chavanne, P., Braissant, O., Picles, U., Gruner, P. and Schumacher, R., 2013. Improvement of mechanical properties of 3D printed hydroxyapatite scaffolds by polymeric infiltration. *Bioceramics Development and Applications*, S1:012.
- Stoia, D.I., Vigar, C. and Rusu, L., 2015. Laser sinterization aspects of PA2200 biocompatible powder – spinal cage application. *Key Engineering Materials*, 638, pp. 352–356.
- Stratasys, 2015. *ULTEM 9085 Resin*. [online] Available at: <<http://www.stratasys.com/materials/fdm/~media/83DA2BBEE7DE4A669CFEF6B1FCA118AA.ashx>> [Accessed September 2015].
- Stratasys, 2016. *PolyJet Technology*. [online] Available at: <<http://www.stratasys.com/3d-printers/technologies/polyjet-technology>> [Accessed February 2016].
- Tao, C.T. and Young, T.H., 2006. Polyetherimide membrane formation by the cononsolvent system and its biocompatibility of MG63 cell line. *Journal of Membrane Science*, 269(1–2), pp. 66–74.
- Tyagi, G., 2011. *Introduction to 3D Printing*. [pdf] Lucknow, Uttar Pradesh, India: National Informatics Centre. Available at: <[nicsu.up.nic.in/knowdesk/3D-Printing-Technology.pdf](https://nicsu.up.nic.in/knowdesk/3D-Printing-Technology.pdf)> [Accessed 12 January 2015].
- Williams, J.M., Adewunmi, A., Schek, R.M., Flanagan, C.L., Krebsbach, P.H., Feinberg, S.E., Hollister S.J. and Das, S., 2005. Bone tissue engineering using polycaprolactone scaffolds fabricated via selective laser sintering. *Biomaterials*, 23(26), pp. 4817–4827.
- Yahamed, A., Ikononov, P., Fleming P.D., Pekarovicova A. and Gustafson, P., 2016. 3D printing of model polymeric resins for medical applications. In: P. Gane, ed. *Advances in Printing and Media Technology: Proceedings of the 43<sup>rd</sup> International Research Conference of IARIGAI*. Toronto, Canada, August 2016. Darmstadt: International Association of Research Organizations for the Information, Media and Graphic Arts Industries. pp. 137–142.
- Yahamed, A., Joyce, M., Fleming, P.D. and Pekarovicova, A., 2015. Biopolymers for 3D printed bone structure. In: *31<sup>st</sup> International Conference on Digital Printing: Digital Fabrication and Digital Printing*. Portland, 27 September to 1 October 2015. Springfield: Society for Imaging Science and Technology. pp. 406–410.

Appendix A

Figures A1 to A9 show the results of tensile strength tests for designed structures (ca is abbreviation for calculated).

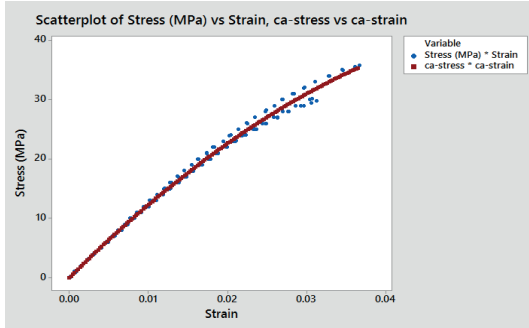


Figure A1: Measured stress-strain and calculated stress-strain of ULTEM9085 hexagonal structure

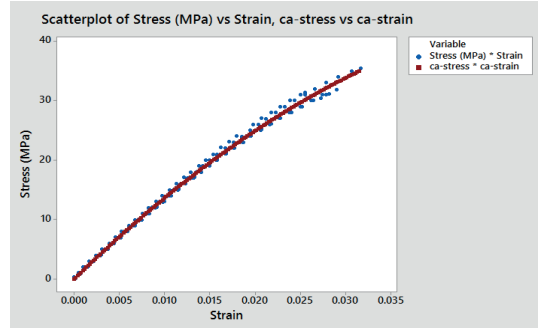


Figure A2: Measured stress-strain and calculated stress-strain of ULTEM9085 triangular structure

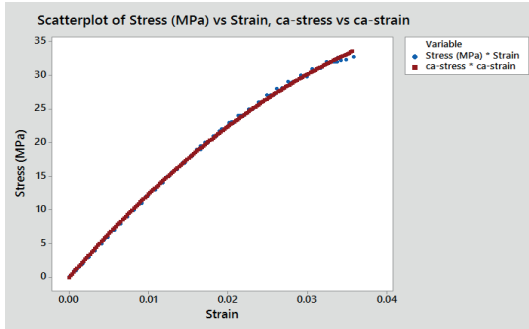


Figure A3: Measured stress-strain and calculated stress-strain of ULTEM9085 square structure

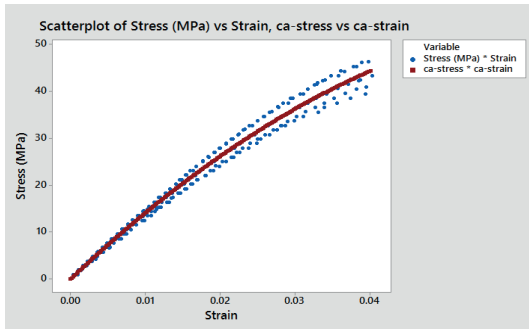


Figure A4: Measured stress-strain and calculated stress-strain of PA2200 hexagonal structure

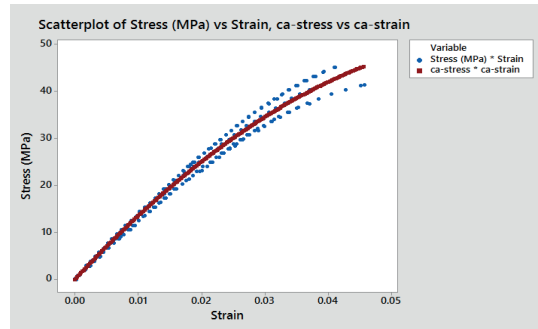


Figure A5: Measured stress-strain and calculated stress-strain of PA2200 triangular structure

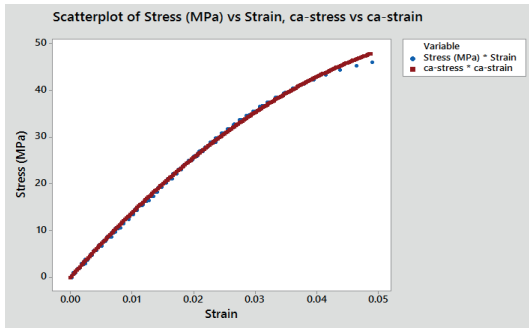


Figure A6: Measured stress-strain and calculated stress-strain of PA2200 square structure

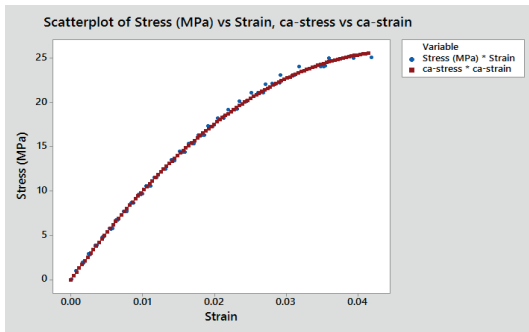


Figure A7: Measured stress-strain and calculated stress-strain of Digital ABS™ hexagonal structure

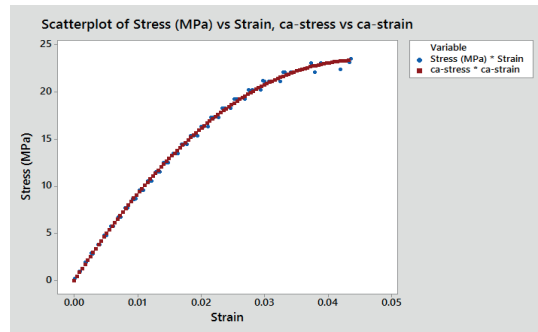


Figure A8: Measured stress-strain and calculated stress-strain of Digital ABS™ triangular structure

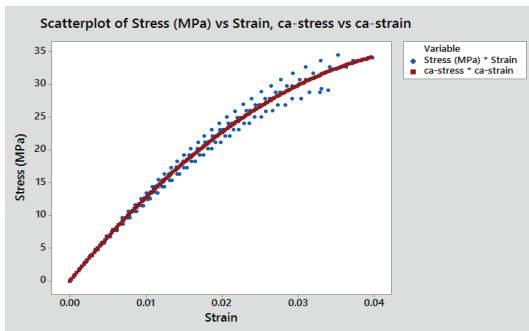


Figure A9: Measured stress-strain and calculated stress-strain of Digital ABS™ square structure

### Appendix B

Figures B1 to B9 show results of the compressive strength tests for designed structures.

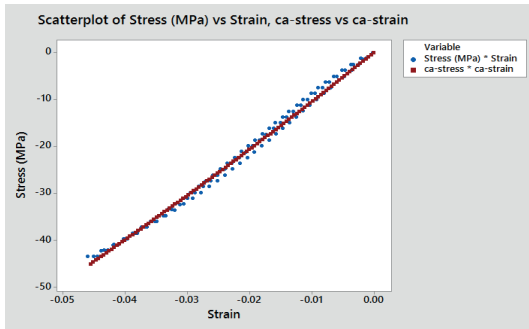


Figure B1: Measured stress-strain and calculated stress-strain of ULTEM9085 hexagonal structure

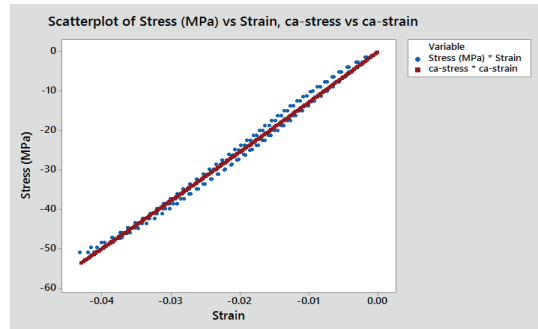


Figure B2: Measured stress-strain and calculated stress-strain of ULTEM9085 triangular structure

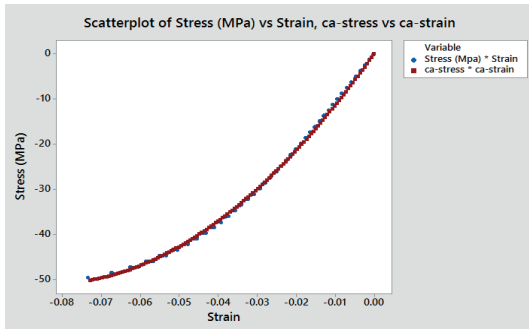


Figure B3: Measured stress-strain and calculated stress-strain of ULTEM9085 square structure

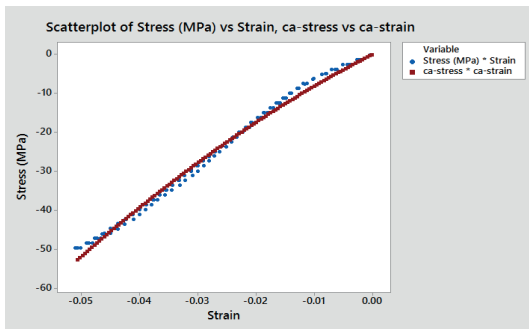


Figure B4: Measured stress-strain and calculated stress-strain of PA2200 hexagonal structure

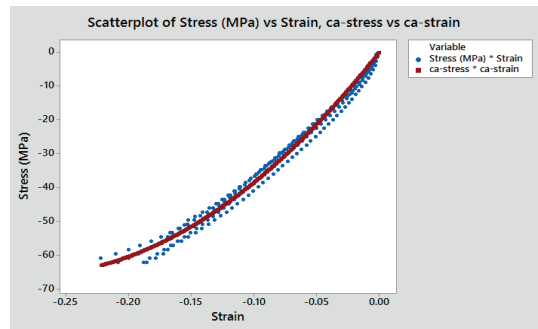


Figure B5: Measured stress-strain and calculated stress-strain of PA2200 triangular structure

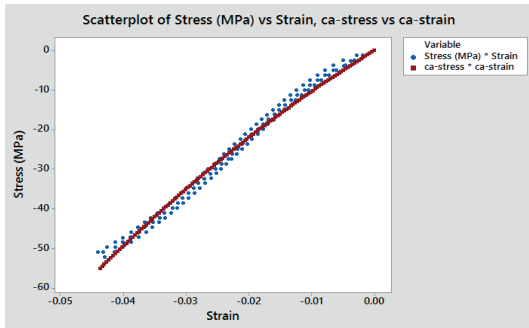


Figure B6: Measured stress-strain and calculated stress-strain of PA2200 square structure

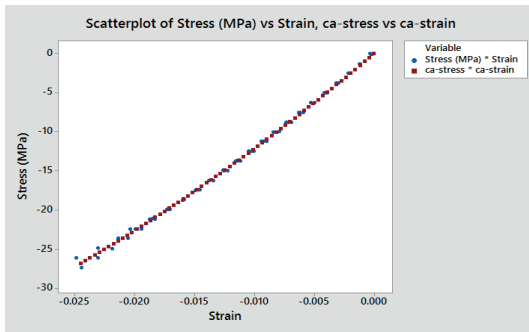


Figure B7: Measured stress-strain and calculated stress-strain of Digital ABS™ hexagonal structure

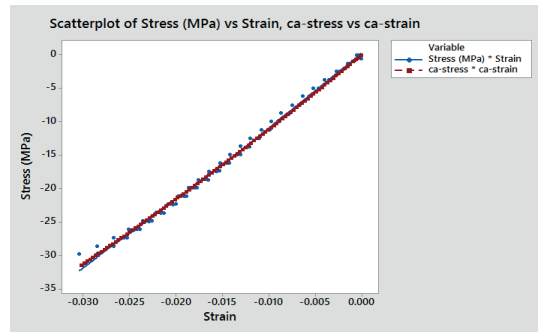


Figure B8: Measured stress-strain and calculated stress-strain of Digital ABS™ triangular structure

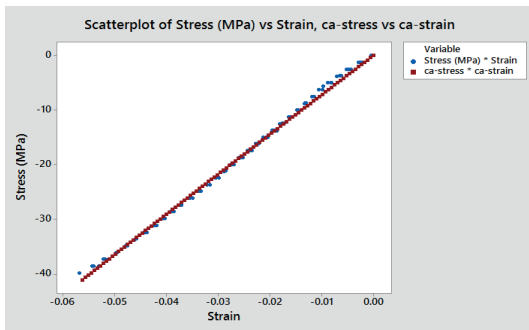


Figure B9: Measured stress-strain and calculated stress-strain of Digital ABS™ square structure

Appendix C

Figures C1 to C9 show results of the bending strength tests for designed structures.

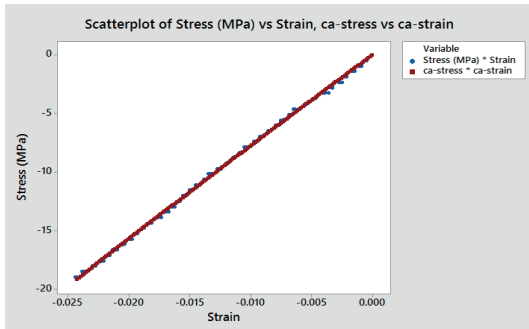


Figure C1: Measured stress-strain and calculated stress-strain of ULTEM9085 hexagonal structure

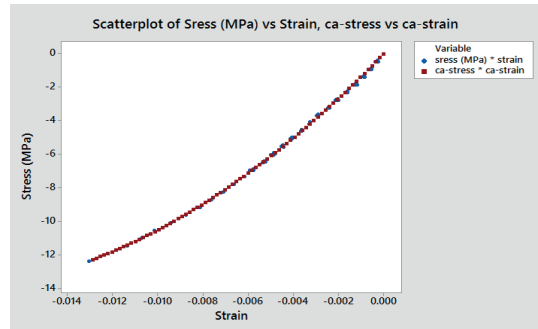


Figure C2: Measured stress-strain and calculated stress-strain of ULTEM9085 triangular structure

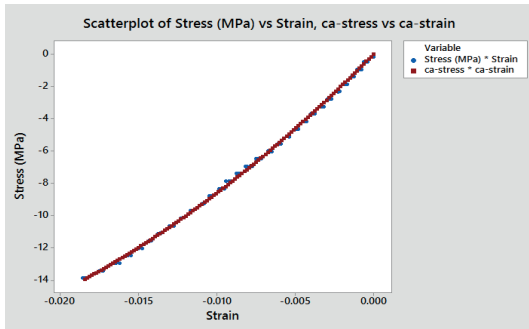


Figure C3: Measured stress-strain and calculated stress-strain of ULTEM9085 square structure

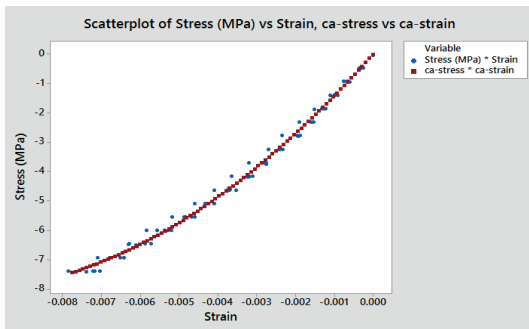


Figure C4: Measured stress-strain and calculated stress-strain of PA2200 hexagonal structure

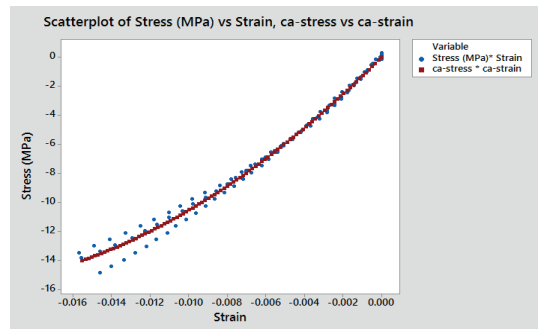


Figure C5: Measured stress-strain and calculated stress-strain of PA2200 triangular structure

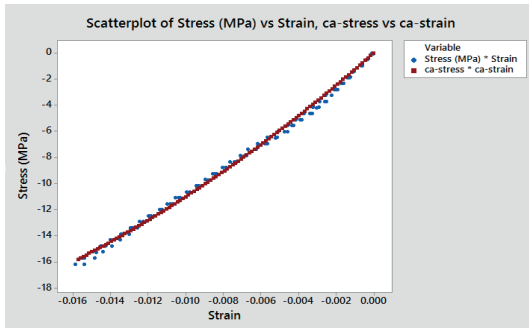


Figure C6: Measured stress-strain and calculated stress-strain of PA2200 square structure

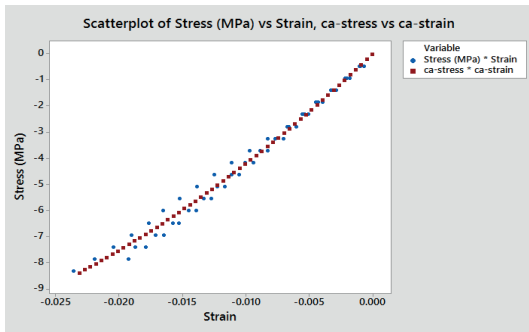


Figure C7: Measured stress-strain and calculated stress-strain of Digital ABS™ hexagonal structure

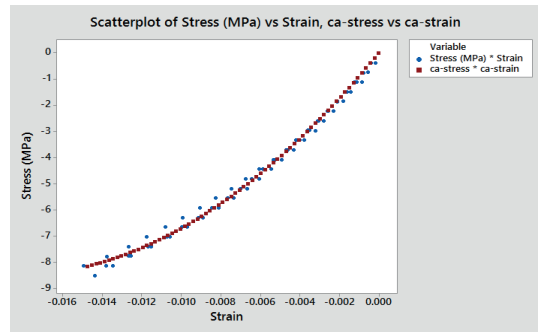


Figure C8: Measured stress-strain and calculated stress-strain of Digital ABS™ triangular structure

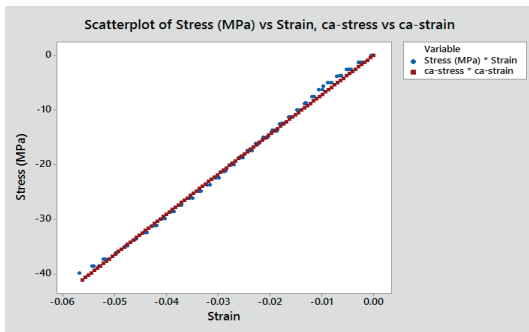


Figure C9: Measured stress-strain and calculated stress-strain of Digital ABS™ square structure

